Identification of beneficial mass-included inerter-based vibration suppression configurations☆

Yi-Yuan Li[a], Sara Ying Zhang[a], Jason Zheng Jiang[a,*], Simon Neild[a]

[a]*Department of Mechanical Engineering, Queen's Building, University Walk, University of Bristol, UK, BS8 1TR*

Abstract

Vibration suppression capabilities of linear passive vibration absorbers, such as traditional tuned mass damper (TMD), and recently proposed inerter-based vibration absorbers, have been studied for multiple mechanical systems. In particular, significant performance advantages have been obtained with a specific device making use of both inerter and mass elements, namely the tuned mass damper inerter (TMDI). However, there are still countless mass-included inerter-based configurations that have not been studied, which can potentially provide more preferred dynamic properties. In this paper, an immittance-function-layout (IFL) is introduced, which can cover a large range of topological connection possibilities with both mass and inerter elements. With the recently proposed structural immittance format, a systematic approach is established to identify the most beneficial IFL type mass-included inerter-based configurations with pre-determined number of each element type. Vibration suppression performance with single-IFL type device and two parallel-connected IFLs (i.e. dual-IFL) type devices are investigated in this paper. Three optimal configurations are identified for mitigating the maximum inter-storey drift of an example 3-storey building model subjected to base excitation. With this 3-storey building model, results show that, for the optimum single-IFL configuration, the performance improvement is 7.3% compared with the optimum TMDI, and with identified beneficial dual-IFL configurations, up to 34.9% performance advantages are obtained. Furthermore, consistent performance gains are shown under real-life earthquake inputs and with a 10-storey building model using identified absorber configurations.

Keywords: Mass-included inerter-based device, Passive vibration control, Immittance-function-layout, Optimum configuration

1. Introduction

The tuned mass damper (TMD), proposed by Frahm [1], is a widely employed passive absorbers consisting of mass, spring and damper elements [2, 3]. To maximize energy dissipation, the tuning method of choosing the damping ratio of the TMD was proposed by Den Hartog [4], which was then refined by others [5, 6, 7, 8]. In most of the real applications, only a single TMD is used and it is always installed near the top of the building, see for example the analysis in [9, 10]. The vibration suppression effectiveness of multiple TMDs has also been investigated by many researchers, for example, in 1984, Iwanami and Seto [11] proposed dual tuned mass dampers (2TMDs) for suppressing the vibration of a single degree of freedom (SDOF) structure with harmonically forced oscillation and it was shown that 2TMDs are more effective than a single TMD. In 2002, a new passive mechanical element termed the inerter has been introduced by Smith [12], which has the property that the generated force is proportional to the relative acceleration across its two terminals. It completes the force-current mechanical-electrical analogy and enables all positive-real functions [13] to be realised by passive networks consisting of inerters, dampers and springs. The performance advantages of various mechanical systems incorporating inerters have been identified, such as automotives [14, 15, 16, 17], railway vehicles [18, 19], landing gears [20] and wind turbines [21, 22]. Many physical realisations of inerters have been proposed and experimentally tested, these include using mechanisms such as a rack-and-pinion [12], a ball-screw [23] and hydraulic implementations [24, 25, 26]. Recently, a novel TMD with an inerter of variable inertance, has been introduced by Brzeski *et al.* [27] and has been shown to be beneficial via theoretical and experimental studies [28, 29]. Apart from pure mechanical absorbers, mechatronic designs, which enable

*Corresponding author
Email address: z.Jiang@bristol.ac.uk (Jason Zheng Jiang)

the controller's immittance to be realised through a combination of mechanical and electrical networks, have also been proposed and shown to be beneficial [30, 31, 32].

Beneficial inerter-based dynamic absorbers have been identified for buildings. Wang *et al.* [33] considered several simple absorber layouts incorporating inerter device which are beneficial in reducing vibration of a one degree of freedom (DOF) and a two DOF building models. In [34], Ikago *et al.* proposed a new seismic control device, the tuned viscous mass damper (TVMD) and analysed the performance of it when installed in a SDOF structure. By replacing the damper of a TMD with a TVMD, a new device, the RIDTMD, was proposed by Garrido *et al.* [35], for which a seismic performance improvement has also been identified. Later on, the tuned inerter damper (TID) [36] was introduced by replacing the mass of the TMD with an inerter, and the seismic performance of it has also been verified by the authors. Despite the fact that there are countless possible network layouts, many other absorbers that might be able to provide better seismic performance has not been investigated. To facilitate the systematic analysis of a large range of possible layouts, the structure-immittance approach was proposed [37], with which generic networks covering a full class of possible series-parallel network layouts with pre-determined number of each element type are formulated. Then corresponding immittance functions, termed as structural immittances can be derived for performance optimisation. Using this approach, both the complexity, the topology and the element values in resulting absorber configurations can be fixed or constraint to be within realistic ranges. However the approach is limited to two terminal elements and no masses can be included.

In [38], a vibration suppression device consisting of an inerter mounted in series with a TMD, termed the tuned mass damper inerter (TMDI), was proposed by Marian and Giaralis and its performance for mitigating seismic vibrations has been investigated [39, 40, 41]. It has been shown that with the same mass, the TMDI can provide superior performance comparing with the TMD. The significant benefits of TMDI demonstrates the potential advantages of mass-included inerter-based devices where all four types of passive mechanical elements, inerters, dampers, springs and masses, are used. The possible topological connections of these four element types are countless. Identification of the most beneficial configurations amongst them is extremely challenging, for which a systematic approach is needed. In this paper, to facilitate such systematic investigations, a mass-included topological connection, labeled the immittance-function-layout (IFL), is introduced. The IFL includes two immittance functions and one reaction mass. Due to the presence of a mass element, the forces generated at the two terminals are not equivalent, therefore an immittance function matrix is first derived to describe these forces in terms of the velocities at the terminals. After that, all distribution possibilities with different types and numbers of elements need to be discussed. Finally, with the element distribution determined, the optimum mass-included inerter-based configurations covered by this IFL can be identified using the structure-immittance approach to determine the two immittance functions, with which, a full class of series-parallel network connections with pre-determined number of inerters, dampers and springs can be efficiently characterised. To investigate the performance effectiveness of two mass-included absorbers, two parallel-connected IFLs (i.e. dual-IFL) with two reaction masses will also be studied in this work.

This paper is arranged as follows. In Section 2, we introduce an example building model, the objective function and the performance comparison between several typical vibration suppression devices. Then the single-IFL and dual-IFL devices are proposed. In Section 3, a systematic approach incorporating the single-IFL type device is demonstrated to identify the optimum configuration for the cases with different pre-determined non-mass element numbers. Dual-IFL type device is investigated in Section 4 by using the systematic approach, where several beneficial configurations are identified. Then the identified optimum configurations are tested under the real-life earthquake excitations. A 10-storey building model is also employed to further verify the effectiveness of the proposed systematic approach. Finally, conclusions are drawn in Section 5.

2. Introduction of the building model, the performance criteria and the immittance-function-layout

2.1. Three-storey building model and the performance criteria

In this paper, firstly a 3-storey structure, modelled as a lumped mass system is shown in Figure 1(a), incorporating one of three vibration suppression devices, namely, the TMD, the TID and the TMDI, as shown in Figures 1(b)-(d). The study is then extended in Section 3 and 4 to incorporate a generic suppression device that potentially incorporates mass element. Floor mass and inter-storey stiffness of the 1st, 2nd and 3rd floor are denoted as M_1, M_2, M_3, and k_{s1}, k_{s2}, k_{s3}, respectively. In this paper, the floor mass is taken to be $M_1 = M_2 = M_3 = M = 1000\,\text{kg}$ and the inter-storey stiffness is

$k_{s1} = k_{s2} = k_{s3} = k_s = 1500\,\text{kN/m}$. The structural damping is taken to be zero since it is typically small compared with that of the control device, following [36, 37]. The vibration suppression device is located between the 2nd and 3rd floor, where F_u and F_l represents the force exerted by the vibration suppression device to the upper floor and the lower floor, respectively.

The equations of motion for this 3-storey building model integrating the vibration absorber can be represented by Equation (1) in Laplace domain:

$$\begin{bmatrix} M & 0 & 0 \\ 0 & M & 0 \\ 0 & 0 & M \end{bmatrix} \begin{bmatrix} s^2X_1(s) \\ s^2X_2(s) \\ s^2X_3(s) \end{bmatrix} + \begin{bmatrix} 2k_s & -k_s & 0 \\ -k_s & 2k_s & -k_s \\ 0 & -k_s & k_s \end{bmatrix} \begin{bmatrix} X_1(s) \\ X_2(s) \\ X_3(s) \end{bmatrix} = \begin{bmatrix} k_sR(s) \\ -F_l \\ F_u \end{bmatrix} \tag{1}$$

where $X_1(s)$, $X_2(s)$, $X_3(s)$ and $R(s)$ are displacements of different floors and the ground, respectively.

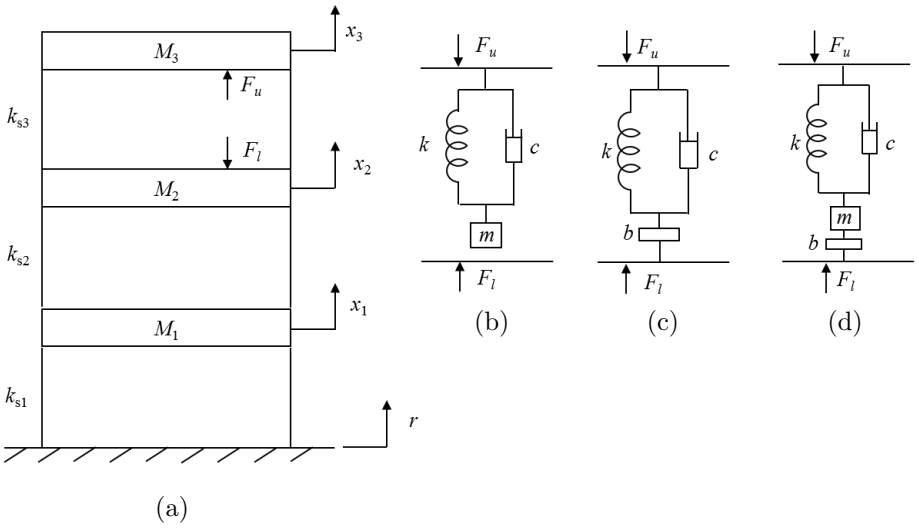

Figure 1: (a) An example 3-storey building model with typical vibration suppression devices, including (b) TMD (c) TID and (d) TMDI.

In this work, we consider the inter-storey drift displacements, accounting for the seismic damage of the building model, as the performance index. The inter-storey drift is denoted as X_{di} with $i = 1, 2, 3$ in Laplace domain, $X_{di}(s) = X_i(s) - X_{i-1}(s)$ with $X_0(s)$ representing the ground displacement $R(s)$. In this way, the inter-storey drift $X_{di}(s)$ can be obtained from Equation (1). With the obtained X_{di}, the objective function is defined:

$$\begin{aligned} &J_\infty = \max\left(\left\|T_{s^2R\to X_{di}}(j\omega)\right\|_\infty\right),\ i = 1, 2, 3 \\ &\text{subjected to: } m = 150\,\text{kg},\ b \in [0, 1000]\,\text{kg} \end{aligned} \tag{2}$$

where $T_{s^2R\to X_{di}}$ denotes the transfer function from ground acceleration $s^2R(s)$ to inter-storey drifts $X_{di}(s)$ and $\|T_{s^2R\to X_{di}}(j\omega)\|_\infty$ is the standard H_∞ norm, which represents the maximum magnitude of $T_{s^2R\to X_{di}}$ across all frequencies. Based on the previous studies [4], the larger the mass value, the better the performance of the TMD. However, in practice, a very large mass is not achievable because of the weight and space constraints. Therefore, in this paper, we fix the mass value to be $m = 150\,\text{kg}$, which is 5% of the whole building mass. On the other hand, inerter can achieve higher inertance value using gearings in mechanical inerters [17] or adjusting the piston-cylinder cross-sectional area ratio in fluid inerters [24, 26, 42]. Hence, in this study, an upper bound of 1000 kg is used to constrain the inertance value b, which is equal to the mass of one floor.

We note that there are many performance criteria adopted for building vibration suppression, such as relative displacement, inter-storey drift, and weighted frequency distributions [43]. The building model used can indeed be more complicated as well. The specific formulation of this mathematical problem serves the purpose of demonstrating the proposed systematic approach. Same procedure specified in this work can be applied to different mechanical systems and performance criteria.

2.2. Performance of three typical layouts

In this sub-section, three typical absorbers are investigated, which are TMD, TID and TMDI, shown in Figures 1(b)-(d). The objective function J_∞ in Equation (2) is optimised to identify the absorber pa-

rameter values using a combination of *patternsearch* and *fminsearch* in Matlab, with *fminsearch* refining the results obtained via *patternsearch*. The same approach is utilised for all the optimisations in this work. We choose to use these because they are effective optimisation tools to find the optimum results, and have been used widely, see for example [18, 21, 44]. Other software with effective genetic optimisation algorithms can also be used for the optimisation procedure. Results for these three devices are summarised in Table 1. It can be seen that with the same added mass, $m = 150\,\text{kg}$, TMDI can provide a 36.6% performance improvement compared with TMD, and it also outperforms TID with 38.8% smaller value of J_∞ using much lower level of inertance. Since the TMDI provides the best performance in this example, it is used as a benchmark for the studies in Sections 3 and 4. Response of the optimum TMD will also be included because this is a very widely studied device. It should be noted that based on the previous studies [36, 44], the TID can achieve better performance than the TMD by mounting it at the bottom of the host building structures along with larger inertance. Figure 2 shows the frequency responses of the three inter-storey drifts $T_{s^2 R \to X_{di}}$ integrating one of the three optimised configurations. It can be observed that the peaks in the first mode natural frequency are split into two peaks for where TID and TMDI are used. However, the TMD splitting peaks are difficult to observe. This is because these peaks are very close together, at 2.54 Hz and 2.63 Hz.

Table 1: Optimisation results using TMD, TID and TMDI layouts

Optimum configurations	J_∞	k (kN/m)	c (kNs/m)	$b \in [0, 1000]$ (kg)
TMD	0.0172	38.76	1.71	/
TID	0.0178	354.14	4.47	1000
TMDI	0.0109	59.38	1.27	80.16

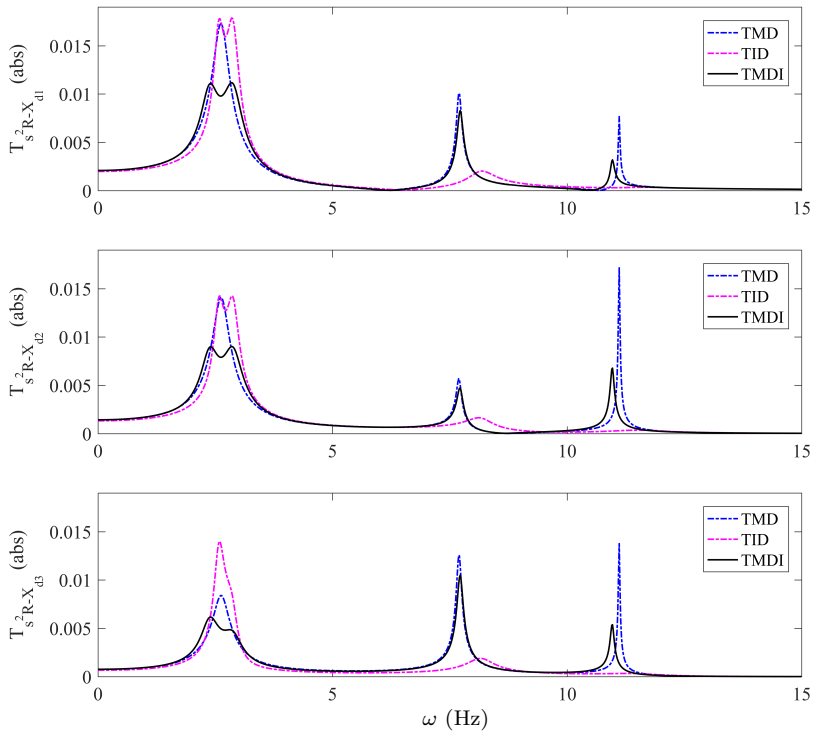

Figure 2: Frequency response comparison of the building structure inter-storey drifts with optimum TMD, TID and TMDI.

2.3. Immittance-function-layout

In Section 2.2, it has been shown that for the structure considered here, the TMDI is more effective in mitigating the seismic vibration comparing with the TMD and TID. In order to identify beneficial mass-

included inerter-based absorber configurations, an immittance-function-layout (IFL) is proposed. This is a specific network layout with immittance functions included, where the immittance function represents sub-network consisting of springs, dampers and inerters. The proposed IFL is shown in Figure 3, where $Y_i(s) = F_i(s)/V_i(s)$ with $i = u, l$. $Y_u(s)$ and $Y_l(s)$ are the force-velocity passive mechanical immittance representing a sub-network, which consists of non-mass elements only, and connects to the upper and lower floor, respectively. $F_u(s)$, $F_l(s)$ are the forces exerted by the corresponding sub-networks, and $V_u(s)$, $V_l(s)$ are the relative velocities across their two terminals. Note that although the topological connection of the added mass is given and fixed in prior, different numbers of degrees-of-freedom (DOFs) will be introduced for different layouts. When elements or sub-networks are connected in series, extra DOFs are introduced.

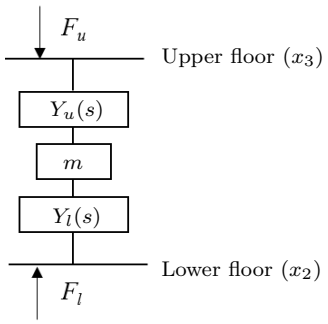

Figure 3: Proposed single-IFL type mass-included inerter-based device.

Since mass is included in the IFL device, the forces F_u and F_l exerted on the two corresponding floors are not equal in magnitude. They are related to the displacements $X_2(s)$ and $X_3(s)$ and the immittance function matrix is give as:

$$\begin{bmatrix} F_l \\ F_u \end{bmatrix} = \begin{bmatrix} -\dfrac{Y_l(s)(ms^2 + sY_u(s))}{ms + Y_l(s) + Y_u(s)} & \dfrac{sY_u(s)Y_l(s)}{ms + Y_u(s) + Y_l(s)} \\ -\dfrac{sY_l(s)Y_u(s)}{ms + Y_u(s) + Y_l(s)} & \dfrac{Y_u(s)(ms^2 + sY_l(s))}{ms + Y_u(s) + Y_l(s)} \end{bmatrix} \begin{bmatrix} X_2(s) \\ X_3(s) \end{bmatrix} \tag{3}$$

Using the immittance matrix as in Equation (3), forces F_l and F_u exerted by a full set of IFL-type vibration suppression devices can be obtained. Taking the TMDI as an example, we have $Y_u = k/s + c$ and $Y_l = bs$. It should be noted that the proposed IFL also covers special cases like the TMD, where Y_l or Y_u equals 0, and the TID, where $m = 0$ and $Y_l = \infty$. With $Y_u = k/s + c$ and $Y_l = 0$, the forces exerted by TMD are $F_u = ms^2Y_u(s)X_3(s)/(ms + Y_u(s))$, $F_l = 0$; for TID, $Y_u = 1/(1/(bs) + 1/(k/s + c))$, $Y_l = \infty$ and $m = 0\,\text{kg}$, therefore, $F_l = F_u = sY_u(X_3 - X_2)$.

It has been shown by previous researchers (e.g. in [11]) that multiple TMDs are more effective than a single TMD for vibration suppression. To this end, two parallel-connected IFL layout, which is termed as a dual-IFL device, is proposed, as shown in Figure 9 in Section 4. Identification of beneficial single-IFL and dual-IFL type devices will be discussed in Section 3 and 4, respectively.

3. Identification of optimum configurations with a single mass-included inerter-based device

In this section, a systematic approach for optimum configuration identification is introduced for a single-IFL type device. Performances of obtained single-IFL configurations are analysed in detail.

3.1. Non-mass element distribution possibilities in the upper and lower sub-networks

Without loss of generality, assuming there are totally n number of non-mass elements in a single-IFL device, it can be denoted as $\text{IFL}_{im(n-i)}$, shown as the top layout of Figure 4. The subscripts i and $(n-i)$ represent the number of non-mass elements contained in the upper and lower sub-networks, respectively. $Y_{u,i}(s)$ is the structural immittance of the upper sub-network with i non-mass elements, and $Y_{l,(n-i)}(s)$ represents the structural immittance of the lower sub-network with $(n-i)$ non-mass elements. It should be noted that both $Y_{u,i}(s)$ and $Y_{l,(n-i)}(s)$ can be an open connection where the immittance function equals 0, or a rigid connection where the immittance function equals ∞. For both cases, the sub-network

contains no element, and we denote as $i = 0$ (for open connection) and $i = \infty$ (for rigid connection). Hence, there are $n+3$ element distribution possibilities in total, which are denoted as $\mathrm{IFL}_{\infty mn}$, IFL_{0mn}, $\mathrm{IFL}_{1m(n-1)}$,..., $\mathrm{IFL}_{im(n-i)}$,..., $\mathrm{IFL}_{(n-1)m1}$, IFL_{nm0}, and $\mathrm{IFL}_{nm\infty}$, as shown in Figure 4. After the number of non-mass elements in each sub-network is determined, the structure-immittance method is adopted to cover the full set of series-parallel topological connection possibilities. An example of how the structure-immittance method is applied will be discussed in detail in Section 3.2.

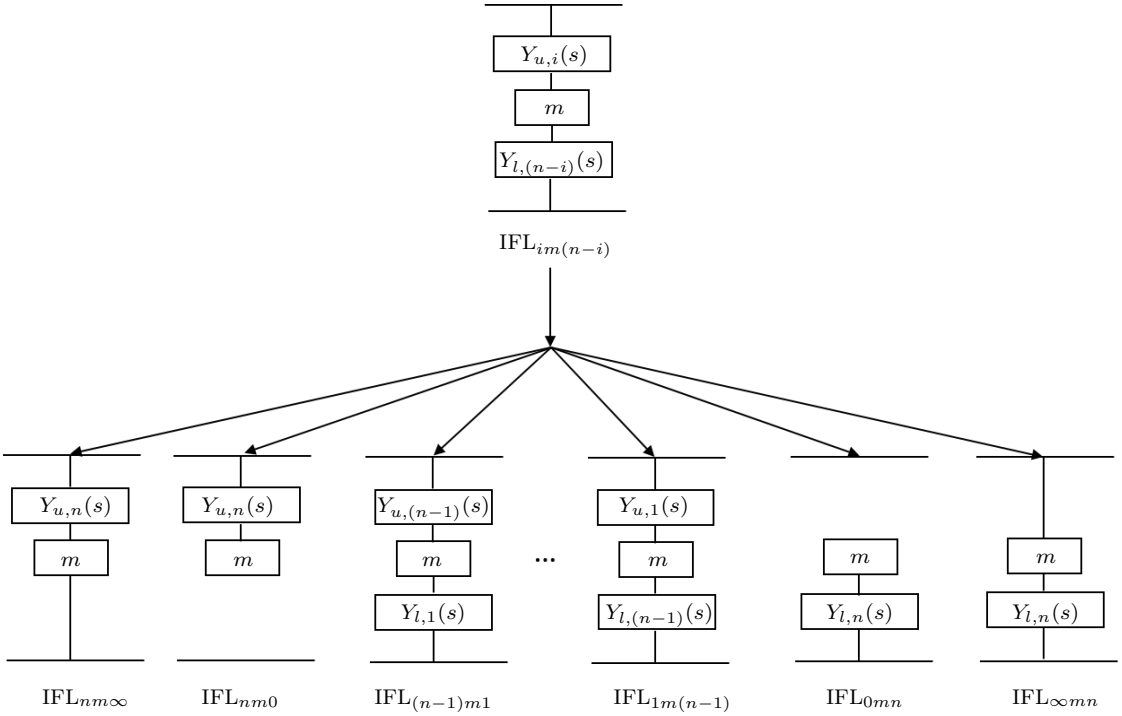

Figure 4: All element distribution possibilities for single-IFL with n non-mass elements.

3.2. Application of the structure-immittance format for single-IFL devices

Regarding the number of each non-mass element type, three cases are considered for single-IFL device. These are Case I: 1 spring, 1 damper and 1 inerter combination, denoted as 1k1c1b case; Case II: 2 springs, 1 damper and 1 inerter combination, denoted as 2k1c1b case; and Case III: 1 spring, 2 dampers and 1 inerter combination, denoted as 1k2c1b case. We will use Case II to explain in detail how the systematic approach is conducted.

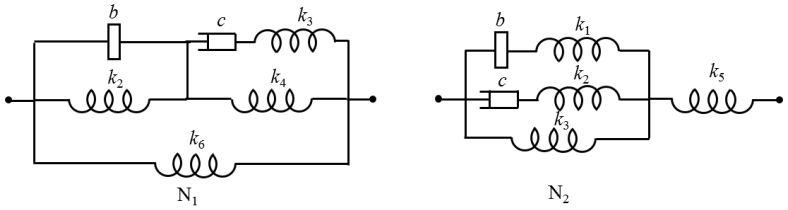

Figure 5: The generic networks obtained based on [37] for Case II where $Y_{u,3}(s)$ contains 1 spring, 1 damper and 1 inerter.

For Case II, there are 7 non-mass distribution possibilities, which are $\mathrm{IFL}_{4m\infty}$, IFL_{4m0}, IFL_{3m1}, IFL_{2m2}, IFL_{1m3}, IFL_{0m4} and $\mathrm{IFL}_{\infty m4}$. Now we use IFL_{3m1} as an example to demonstrate how the structure-immittance method is employed. Three possible combinations of elements in $Y_u(s)$ can be obtained and the remaining one element will be in $Y_{l,1}(s)$. These three combinations are 2 springs and 1 damper (termed as 2k1c); 2 springs and 1 inerter (termed as 2k1b); 1 spring, 1 damper and 1 inerter (termed 1k1c1b). For the 1k1c1b combination, two generic networks, shown as N_1 and N_2 of Figure 5 can be obtained based on the structure-immittance method [37], for which the immittance functions can

be derived as Equation (4),

$$Y_1(s) = \frac{bcs^2 + b(k_4 + k_6)s + c(k_2 + k_6)}{bc(1/k_3)s^3 + bs^2 + cs + k_2 + k_4}$$
$$Y_2(s) = \frac{bc(1/k_1 + 1/k_2)s^3 + bs^2 + cs + k_3}{b(1/k_1 + 1/k_5)s^3 + c(1/k_2 + 1/k_5)s^2 + s} \tag{4}$$

which cover all the possible combinations of one spring, one damper and one inerter. It should be noted that since at most one spring of the networks shown in Figure 5 is present, for $Y_1(s)$ in Equation (4), at least three of the parameters k_2, $1/k_3$, k_4, k_6 must be equal to zero, and for $Y_2(s)$, at least three of the parameters $1/k_1$, $1/k_2$, k_3, $1/k_5$ must be equal to zero. For the combinations of 2k1c and 2k1b, two generic network will suffice. Therefore, the optimisation will be conducted 4 times for the IFL_{3m1} layout. For $\text{IFL}_{4m\infty}$, IFL_{4m0}, IFL_{2m2}, IFL_{1m3}, IFL_{0m4} and $\text{IFL}_{\infty m4}$, the structural immittances can be obtained by following the similar procedure. It can be calculated that 8 generic networks (and the corresponding structural-immittances) will be needed for Case II, which can cover 104 layouts in total. Indeed, as the total number of elements becomes larger, there will be more candidate network layouts, which will lead the proposed approach more complicated. However, the significance of this approach is that it is systematic, which makes it easier to analyse all the possible absorbers; and by making use of the structure-immittance approach, significantly less implementations are needed for the optimisation. Without this proposed systematic approach, it is firstly difficult to enumerate all the possible candidate layouts and secondly hard to take all these layouts into consideration for the optimisation. Furthermore, this approach can potentially be implemented as a computer algorithm, for which the distribution of element types and numbers can be directly obtained. We anticipate that there will be some redundancy in the resulted network, but this will not affect the optimisation results, although there might be more than one minima of cost function that result in identical configurations once the redundancy is noted.

3.3. Optimisation results

Following the above systematic approach, the optimisation procedure is conducted using the structural immittances such as $Y_1(s)$ and $Y_2(s)$ in Equation (4). The results are summarised in Table 2. For Case I and Case III, the most beneficial configuration is the TMDI with the parameter values shown in Table 1. For Case II, the most beneficial configuration is shown in Figure 6, termed C1, with the objective function value $J_\infty = 0.0101$ using the parameter values shown in Table 2. The C1 configuration improves the performance by 7.3% and 41.3% compared with the TMDI and TMD, respectively. Note that two more DOFs (x_1 and x_2) are added when attaching the C1 absorber to the main system, as shown in Figure 6. Besides, C1 only has one attachment point to the hosting structure, so it will also be less affected by the effects such as brace stiffness and backlash compared to the TMDI.

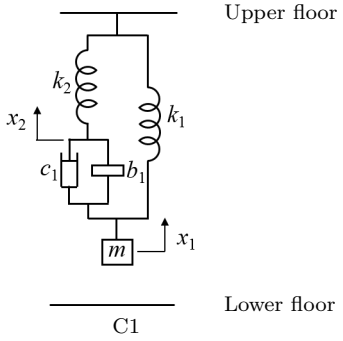

Figure 6: The optimum configuration C1 of the single-IFL type device obtained from Case II, with which two more DOFs are added to the building system.

Figure 7 shows the frequency responses of the three inter-storey drifts $T_{s^2R \to X_{di}}$ integrating the optimum configuration C1, together with the optimum TMD and TMDI. Considering the internal resonance of the device alone, the resonant frequencies for C1 are 3.72 Hz and 6.53 Hz, which target the vicinity of the first and second modes of the main structure, respectively. It can be seen from Figure 7 that, the

Table 2: Optimisation results using the single-IFL type device for Cases I, II and III

Case	optimum configuration	J_∞	improvement compared with the TMDI	k_1 (kN/m)	k_2 (kN/m)	c_1 (kNs/m)	$b_1 \in [0, 1000]$ (kg)
I (1k1c1b)	TMDI	0.0109	/	59.38	/	1.27	80.16
II (2k1c1b)	C1	0.0101	7.3%	89.14	41.86	0.81	23.91
III (1k2c1b)	TMDI	0.0109	/	59.38	/	1.27	80.16

peaks at the vicinity of the first model natural frequency are further reduced by using the C1 configuration, compared with both optimum TMD and TMDI configurations. Peaks for the second and third modes are also effectively suppressed.

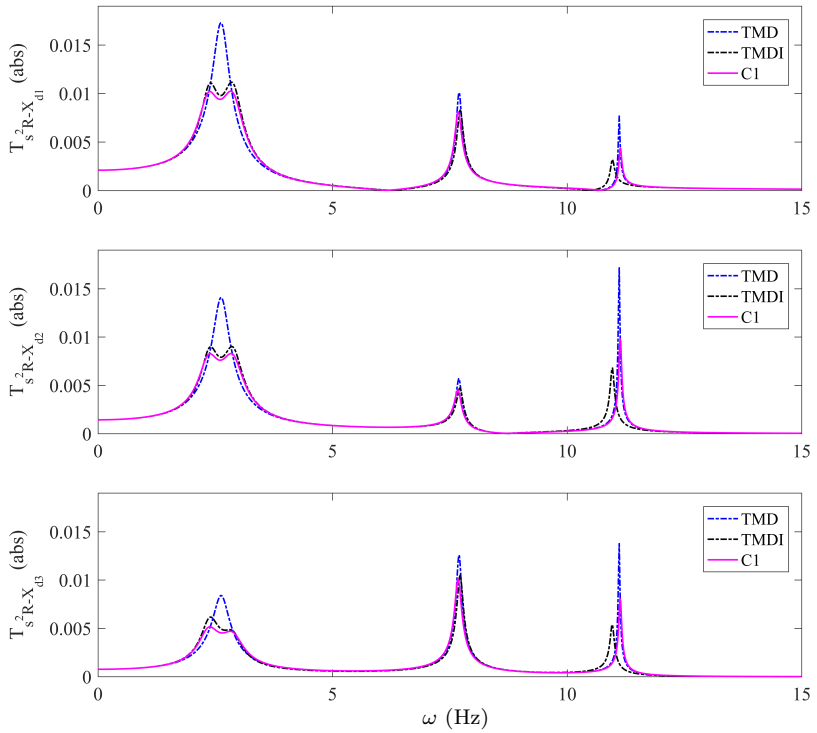

Figure 7: Frequency response comparison of the building structure inter-storey drifts with the optimum TMD, TMDI and C1 configurations.

The effect of the inerter's size on the performance, J_∞, of the main structure with configuration C1, is shown in Figure 8. It can be observed that the optimum performance occurs when $b = 23.91$ kg and as the value of b increases from this, J_∞ becomes larger. This is because the movement between the two terminals across the damper c_1 is diminished as the inerter's size becomes larger. In the extremism when b is infinite, the damper is effectively locked. Furthermore, it can be calculated that, in order to achieve the same level of performance as C1, $J_\infty = 0.0101$, the mass of the TMD and TMDI needs to be increased by 1.83 and 1.74 times of the original value, $m = 150$ kg, respectively. Also for TID, it can be calculated that the inertance value needs to be 133 times compared with that of C1 as shown in Table 2 to match its performance.

4. Identification of optimum configurations with two mass-included inerter-based devices

This section demonstrates how the systematic approach can be applied when a dual-IFL device is used. Performances of obtained dual-IFL configurations are also analysed in detail.

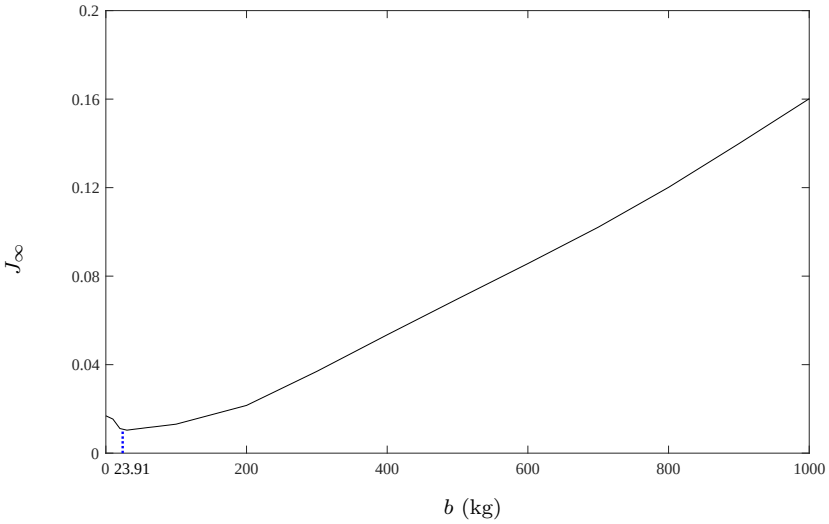

Figure 8: Relationship of performance index J_∞ with respect to different inertance of C1.

4.1. Non-mass element distribution possibilities in a dual-IFL device

A dual-IFL containing n non-mass elements is proposed in Figure 9, where n_1 and n_2 are the number of non-mass elements contained in the left IFL and right IFL of the dual-IFL device, respectively, with $n_1+n_2 = n$. It should be noted that when $n_1 = 0$ or $n_2 = 0$, the dual-IFL device will be reduced to single-IFL device, which has been discussed in Section 3. This dual-IFL is denoted as $\text{IFL}_{im_1(n_1-i),(jm_2(n_2-j))}$. Here, $YL_{u,i}(s)$ and $YL_{l,(n-i)}(s)$ are the structural immittances of the upper and lower sub-networks in the left IFL, which contains i and $(n_1 - i)$ non-mass elements, respectively. Similarly, $YR_{u,j}(s)$ and $YR_{l,(n-j)}(s)$ are the structural immittances of the upper and lower sub-networks in the right IFL, which contains j and (n_2-j) non-mass elements, respectively. Following a similar procedure to that presented in Section 3, all the non-mass elements distribution possibilities for the dual-IFL device can be enumerated. For simplicity, this procedure is not presented in detail. After the element number is determined for each sub-network, the structure-immittance method will be adopted to include all the possible configurations for optimisation. In this section, the total mass value is chosen as $m_1 + m_2 = 150$kg. The inertance value is chosen as $b \leq 1000$kg, in consistency with the rest of the paper.

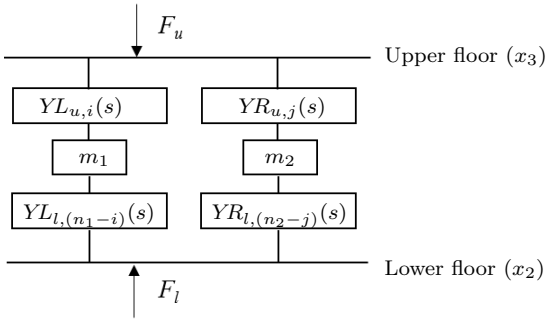

Figure 9: The dual-IFL type devices containing n non-mass elements, where $n_1 + n_2 = n$.

4.2. Optimisation results

Three cases are considered in this section, which are Case IV: 2 springs, 1 damper and 1 inerter combination, denoted as 2k1c1b case; Case V: 1 spring, 2 dampers and 1 inerter combination, denoted as 1k2c1b case; Case VI: 2 springs, 2 dampers and 1 inerter combination, denoted as 2k2c1b case. To constrain the computational complexity, here we limit the element number in each sub-network in Figure 9 to be no more than 4. By conducting the proposed systematic method, the optimum configurations are obtained, with the newly identified ones shown in Figure 10. The corresponding parameter values are summarised in Table 3. For Case IV, the optimum configuration is C1, same as the optimum configuration identified in Section 3. The reason we cannot get a better performance configuration is that there is

only 1 damper, which means one of the IFL device is un-damped. The most beneficial configurations for Case V and Case VI are C2 and C3, respectively. Note that C2 introduces one additional DOF and C3 introduces two extra DOFs to the main system, which are shown in Figures 10(a) and (b). C2L and C2R represent the network configuration at the left and right hand side of C2, and same notation is used for C3. It can be seen that the layouts for both C2L and C3L are TMD. For C2, the objective function is $J_\infty = 0.0079$, and for C3 is $J_\infty = 0.0071$, with the corresponding parameter values for both shown in Table 3.

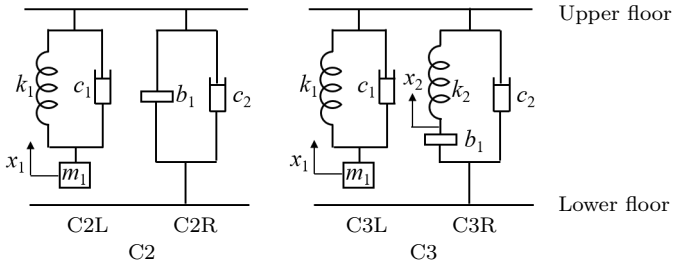

Figure 10: The identified optimum configurations C2 and C3 of dual-TFLs devices from Case V and Case VI, and the extra DOFs they introduce to the building system.

Table 3: Optimisation results using a dual-IFL device for Cases IV, V and VI

Case	Optimum configuration	J_∞	Improvement compared with the TMDI	k_1 (kN/m)	k_2 (kN/m)	c_1 (kNs/m)	c_2 (kNs/m)	$b_1 \in [0, 1000]$ (kg)
IV (2k1c1b)	C1	0.0101	7.3%	89.14	41.86	0.81	/	23.91
V (1k2c1b)	C2	0.0079	27.5%	37.80	/	0.89	45.26	1000
VI (2k2c1b)	C3	0.0071	34.9%	35.27	589.46	0.86	37.37	1000

Figure 11 shows the frequency responses for C2 and C3, together with those for the optimum TMD and TMDI. It can be seen that significant performance advantages have been obtained. Considering the internal resonance of the device alone, for C2, there is only one frequency located at 2.40 Hz. Similar to a TMD, this is close to the first building natural frequency. Therefore the peaks of the first building natural frequency is split into 2 when the full system is considered, which are located at $f_1 = 2.32$ Hz and $f_2 = 2.97$ Hz, respectively. Two frequencies of C3 are 2.44 Hz and 3.86 Hz, both of which target the building's first mode. As a result, the peaks in the first mode natural frequency are split into 3 frequencies, which are $f_1 = 2.25$ Hz, $f_2 = 2.89$ Hz and $f_3 = 3.38$ Hz, all around the first natural frequency of the building model. By comparing the responses of TMDI and C2, which are the optimum results from the 1k2c1b case by using single-IFL device and dual-IFL device, respectively, it can be seen that dual-IFL device significantly outperforms the single-IFL device. Figures 12(a) and (b) present the frequency responses of the first inter-storey drift $T_{s^2R\to X_{d1}}$ for the configuration C2, C2L, C2R and C3, C3L, C3R, by using the optimum parameter values obtained for C2 and C3, respectively. The reason we only choose the first inter-storey drift is because it has the largest response amongst all the three inter-storey drifts. Besides, the trends for $T_{s^2R\to X_{d2}}$ and $T_{s^2R\to X_{d3}}$ are the same as $T_{s^2R\to X_{d1}}$, so are not included for brevity. It it interesting to observe that C2L (resp. C3L) mainly target the first natural frequency, splitting the first mode into two peaks (resp. three peaks), whereas, the second and third modes have not been affected by C2L (resp. C3L). On the other hand, C2R (resp. C3R) alone mainly target the higher modes of the main structure.

Now consider the mass value for a TMD, TID or a TMDI to achieve the same performance as C3, namely $J_\infty = 0.0071$. The mass of the TMD and TMDI needs to be increased by 2.83 and 4.72 times the original $m = 150$ kg, respectively. As for the TID, it is unable to achieve the same performance as C3 even when the inertance value is unconstrained and the minimum $J_\infty = 0.0092$.

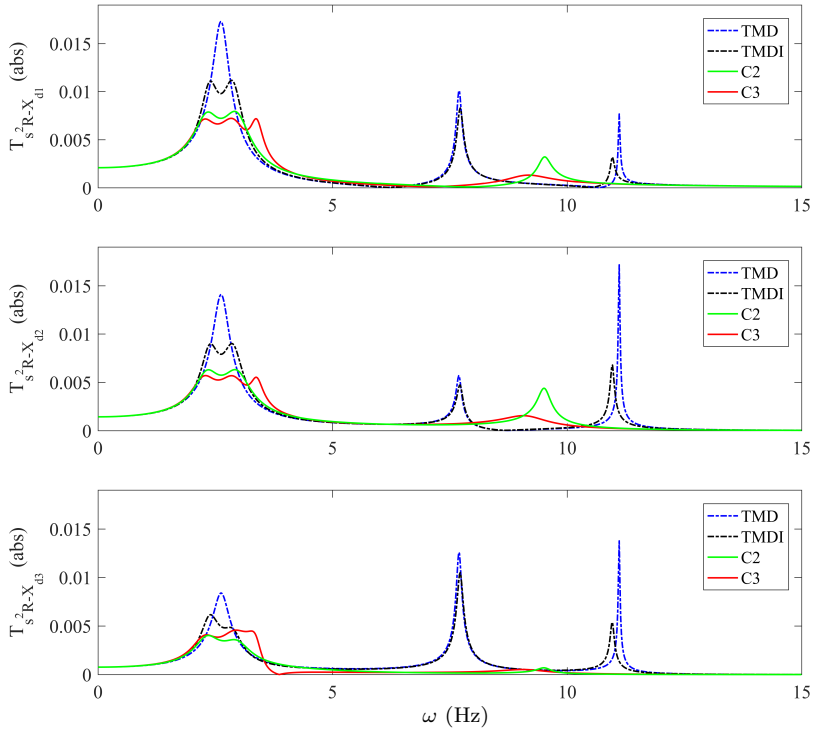

Figure 11: Frequency response comparison of the building structure inter-storey drifts with the optimum TMD, TMDI, C2 and C3 configurations.

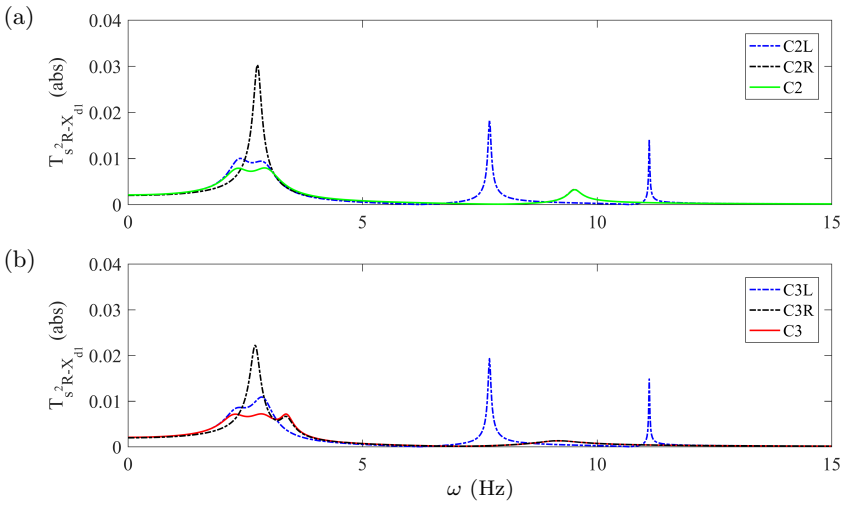

Figure 12: Frequency responses comparison of the building structure inter-storey drift $T_{s^2R\to X_{d1}}$ with (a) C2, C2L, C2R independently; (b) C3, C3L and C3R independently.

4.3. Verification of the obtained beneficial absorbers

Using the identified configurations, the building model's response subjected to two real-life earthquake excitations are examined. One is a 50 second ground acceleration record from the 1995 Kobe earthquake in Japan, with the time history ground acceleration and single-sided Fourier spectrum shown in Figure 13(a) and Figure 14(a), respectively. The other is a recording from the 2011 Tohoku earthquake with a longer duration, see Figure 15(a) and Figure 16(a). Figure 13(b) shows a time history of the inter-storey drift of the first floor relative to the ground under the Kobe earthquake, with the black, blue, green and red lines represent the responses incorporating the optimum configurations TMDI, C1, C2 and C3, respectively. It can be observed that the results of the inter-storey drift time histories responses are consistent with the performance index J_∞, where the performance from best to worst is C3, C2, C1, then the TMDI. Figure 14(b) shows the single-sided Fourier spectrum of the inter-storey drift X_{d1} incorporating the TMDI, C1, C2 and C3, respectively. The highest amplitudes are attained

at low frequencies, hence only the 0-7 Hz frequency ranges is shown. The first natural frequency of the structure is $f_1 = 2.74$ Hz, tuned to match the high amplitude frequency region of the chosen ground motion. The relative displacement time history and the single-sided Fourier spectrum of the inter-storey drift X_{d1} under the Tohoku earthquake are shown in Figure 15(b) and Figure 16(b), respectively. Again, it can be seen that the configuration C3 achieves best seismic performance, followed by C2 and C1, and finally the optimum TMDI.

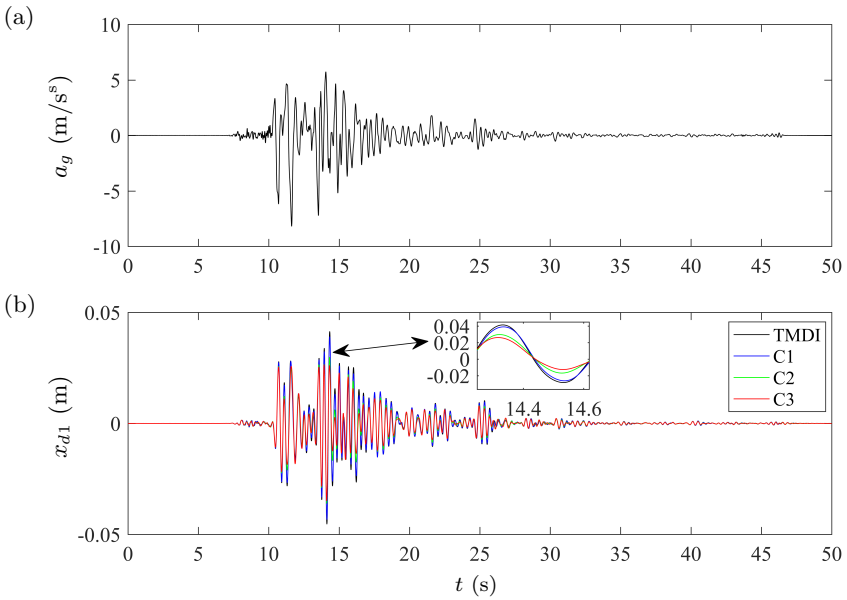

Figure 13: Time-history of (a) ground acceleration; (b) inter-storey drift of the first floor relative to the ground with C1, C2, C3 and optimum TMDI, where the Kobe earthquake input is used.

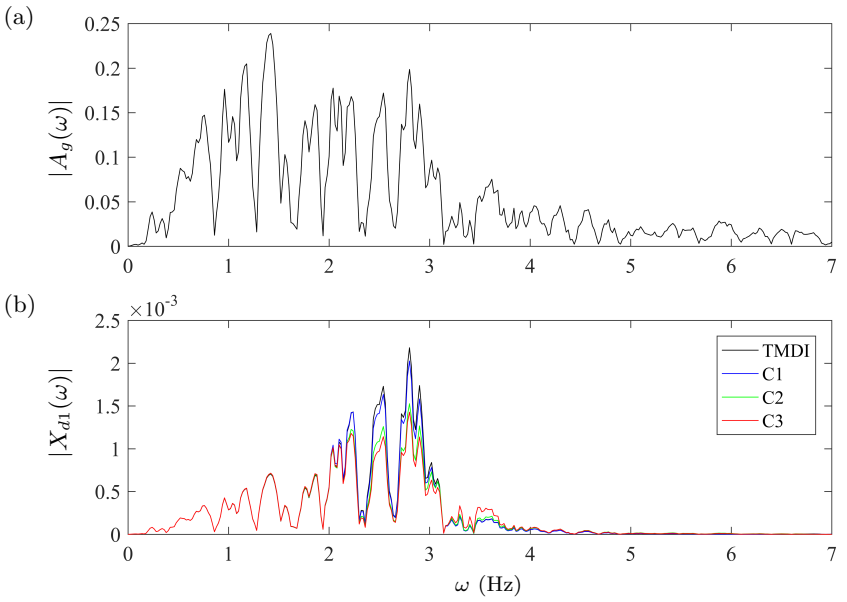

Figure 14: Single-sided Fourier spectra of (a) ground acceleration; (b) inter-storey drift of the first floor relative to the ground with C1, C2, C3 and the optimum TMDI, where the Kobe earthquake input is used.

In order to further verify the effectiveness of this approach, a 10-storey building model subjected to base excitation is now considered, where the floor mass and inter-storey stiffness remain consistent with the 3-storey building, i.e. 1000 kg and 1500 kN/m, respectively. The identified configurations C1, C2 and C3 are re-optimised with the TMD and the TMDI as comparison. Results are shown in Table 4 and Figure 17, from which superior performance can still be obtained by using C1, C2 and C3 on the 10-storey building.

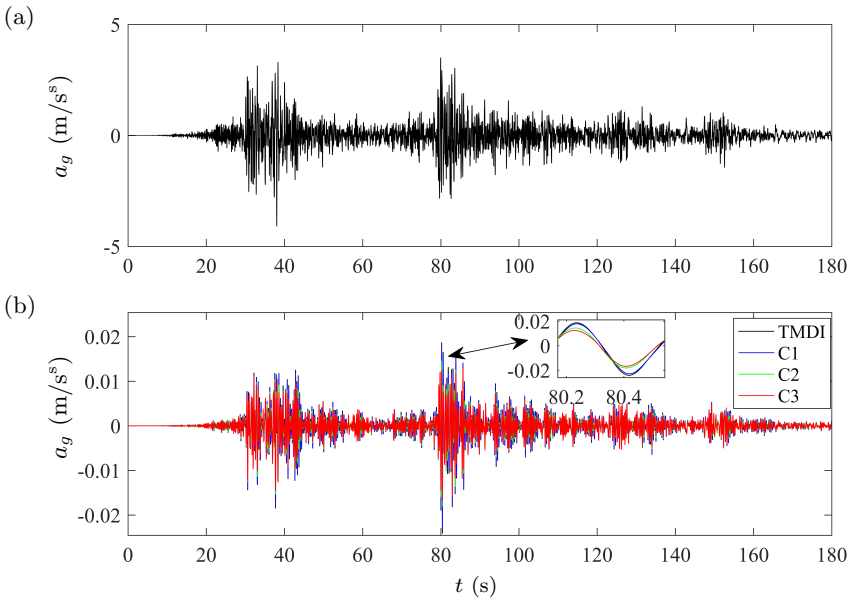

Figure 15: Time-history of (a) ground acceleration; (b) inter-storey drift of the first floor relative to the ground with C1, C2, C3 and optimum TMDI, where the Tohoku earthquake input is used.

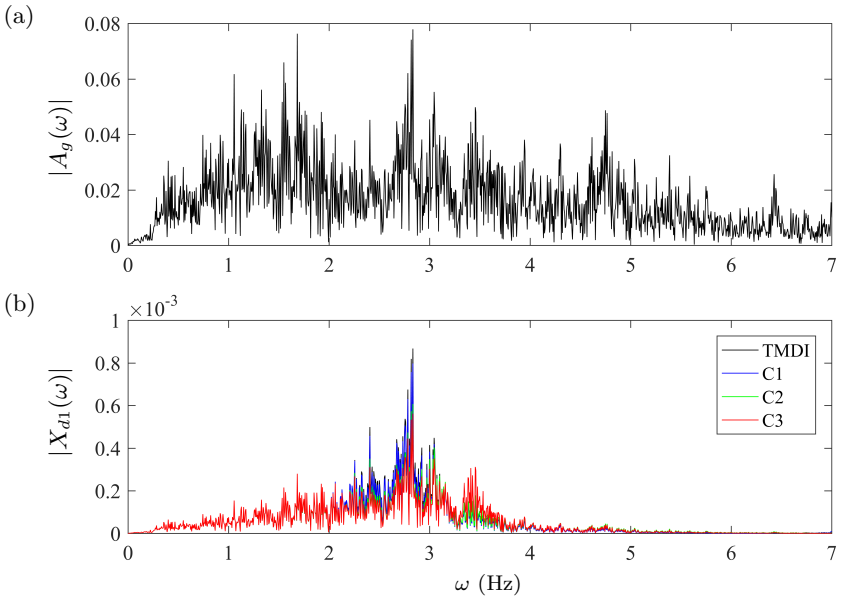

Figure 16: Single-sided Fourier spectra of (a) Ground acceleration; (b) Inter-storey drift of the first floor relative to the ground with C1, C2, C3 and optimum TMDI, where the Tohoku earthquake input is used.

Frequency responses of the first floor inter-storey drift relative to the ground for TMD, TMDI and C3 are shown in Figure 17. Similar as 3-storey building case, frequencies of C3 target the building's first

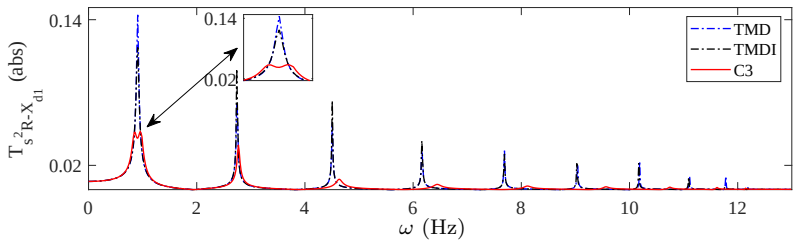

Figure 17: Frequency response of the first floor inter-storey drift relative to the ground for TMD, TMDI and C3 on a 10-storey building model.

Table 4: Optimisation results of TMD, TMDI, C1, C2 and C3 on a 10-storey building model

Optimum configurations	J_∞	Improvements compared with the TMDI	k_1 (kN/m)	k_2 (kN/m)	$c1$ (kNs/m)	$c2$ (kNs/m)	$b \in [0, 1000]$ (kg)
TMD	0.144	/	4.78	/	0.600	/	/
TMDI	0.117	/	54.6	/	0.491	/	18.5
C1	0.106	9.4%	42.9	4.97	0.436	/	7.34
C2	0.048	59.0%	4.74	/	0.175	146.5	1000
C3	0.047	59.8%	4.73	36.7	0.176	86.5	1000

mode, resulting three frequencies in the first mode, i.e. $f_1 = 0.85$ Hz, $f_2 = 0.97$ Hz, $f_3 = 0.98$ Hz. Only two peaks can be observed in the figure, this is because f_2 and f_3 are very close to each other. Note that if the systematic approach is fully adopted where all possible configurations are considered, even more enhanced performance might be achieved.

5. Conclusion

In this paper, an immittance-function-layout (IFL) is proposed, which can cover a large range of one-mass-included inerter-based vibration suppress devices. By using the proposed IFL, a systematic approach has been adopted to identify the most beneficial configurations with pre-determined number of each element type. In order to cover the range of two-mass-included inerter based devices as well as identifying more beneficial configurations, dual-IFL type devices with two parallel-connected IFL layout, are also considered. Three optimal configurations, C1, C2 and C3 which incorporate inerter(s), spring(s), damper(s), as well as mass(es) have been identified for mitigating the maximum inter-storey drift of a three-storey building model structure subjected to base excitation. C1 is a single-IFL type device, whereas C2, C3 are dual-IFL layouts. Responses using configurations C1, C2 and C3, provide improvements of up to 34.9% compared to optimum TMDI. It is also shown that the dual-IFL type devices outperforms the single-IFL devices with same mass constraints. This is because for the identified dual-IFL device, one IFL mainly targets the building's first natural frequency, and the other IFL targets higher frequencies. Finally, real-life earthquake inputs are used on the 3-storey building model incorporating the identified absorbers, which show advantages of those absorbers on mitigating seismic vibrations compared with optimum TMDI. A 10-storey building model subjected to base excitation is also adopted to further verify the effectiveness of the identified absorbers.

6. Acknowledgements

The authors would like to acknowledge the support of the EPSRC and the University of Bristol: Y.-Y.Li is funded by the Deans Scholarship of University of Bristol and the China Scholarship Council; S.Y.Zhang and J.Z.Jiang are supported by the EPSRC grant EP/P013546/1; S.A.Neild is supported by EPSRC fellowship EP/K005375/1.

References

[1] H. Frahm, Device for damping vibrations of bodies, Patent no. US989958A.

[2] T. T. Soong, G. F. Dargush, Passive energy dissipation systems in structural engineering, Chichester, UK:Wiley.

[3] S. Krenk, Frequency analysis of the tuned mass damper, Journal of Applied Mechanics 72 (2005) 936942.

[4] J. D. Hartog, Mechanical vibration, McGraw Hill: York PA, USA,.

[5] Y. Fujino, M. Abe, Design formulas for tuned mass dampers based on a perturbation technique, Earthquake Engineering and Structural Dynamics 22 (1993) 833–854.

[6] C. Moutinho, An alternative methodology for designing tuned mass dampers to reduce seismic vibrations in building structures, Earthquake Engineering and Structural Dynamics 41 (2012) 2059–2073.

[7] M. Angelis, S. Perno, A. Reggio, Dynamic response and optimal design of structures with large mass ratio tmd, Earthquake Engineering and Structural Dynamics 41 (2012) 41–60.

[8] N. Anh, N. Nguyen, Extension of equivalent linearization method to design of tmd for linear damped systems, Structural Control and Health Monitoring 19 (2012) 565–573.

[9] R. Villaverde, Reduction in seismic response with heavily-damped vibration absorbers, Earthquake Engineering and Structural Dynamics 13 (1985) 33–42.

[10] F. Sadek, B. Mohraz, A. Taylor, R. Chung, A method of estimating the parameters of tuned mass damper for seismic applications, Earthquake Engineering and Structural Dynamics 26 (1997) 617–635.

[11] K. Iwanami, K. Seto, Optimum design of dual tuned mass dampers and their effectiveness, Proceedings of the JSME(C) 50 (1984) 44–52.

[12] M. Smith, Synthesis of mechanical networks: the inerter, IEEE Transactions on Automatic Control 47 (2002) 1648–1662.

[13] R. Bott, R. Duffin, Impedance synthesis without use of transformers, Journal of Applied Physics 20 (1949) 816.

[14] C. Papageorgiou, M. Smith, Positive real synthesis using matrix inequalities for mechanical networks: application to vehicle suspension, IEEE Transactions on Control Systems Technology 14 (2006) 423–435.

[15] M. Smith, F. Wang, Performance benefits in passive vehicle suspensions employing inerters, Vehicle System Dynamics 42 (2004) 235–247.

[16] M. Chen, C. Papageorgiou, F. Scheibe, F. C. Wang, M. Smith, The missing mechanical circuit element, IEEE Circuits and Systems Magazine 9 (2009) 10–26.

[17] M. Smith, http://www.eng.cam.ac.uk/news/stories/2008/mclaren [19 August,2008].

[18] F. C. Wang, M. K. Liao, B. H. Liao, W. J. Su, H. A. Chan, The performance improvements of train suspension systems with mechanical networks employing inerters, Vehicle System Dynamics 47 (2009) 805–830.

[19] J. Z. Jiang, A. Matamoros-Sanchez, R. Goodall, M. Smith, Passive suspensions incorporating inerters for railway vehicles, Vehicle System Dynamics 50 (2011) 263–276.

[20] Y. Li, J. Z. Jiang, S. Neild, Inerter-based configurations for main landing gear shimmy suppression, Journal of Aircraft (2016) 684–693.

[21] Y. Hu, M. Chen, Inerter-based passive structural control for load mitigation of wind turbines, 29th Chinese Control And Decision Conference (CCDC) (2009) 17040818.

[22] Y.-Y. Li, S. Y. Zhang, J. Z. Jiang, S. Neild, I. Ward, Passive vibration control of offshore wind turbines using the structure immittance approach, International Conference on Noise and Vibration Engineering.

[23] C. Papageorgiou, N. E. Houghton, M. C. Smith, Experimental testing and analysis of inerter devices, Journal of Dynamic System 131 (2009) 011001–1.

[24] S. Swift, M. Smith, A. Glover, C. Papageorgiou, B. Gartner, N. Houghton, Design and modelling of a fluid inerter, International Journal of Control 86 (2013) 2035–2051.

[25] F. C. Wang, M. F. Hong, T. C. Lin, Designing and testing a hydraulic inerter, Journal of Mechanical Engineering Science 225 (2011) 66–72.

[26] X. Liu, J. Jiang, B. Titurus, A. Harrison, Model identification methodology for fluid-based inerters, Mechanical Systems and Signal Processing 106 (2018) 479–494.

[27] P. Brzeski, T. Kapitaniak, P. Perlikowski, Novel type of tuned mass damper with inerter which enables changes of inertance, Journal of Sound and Vibration 349 (2015) 56–66.

[28] P. Brzeski, M. Lazarek, P. Perlikowski, Experimental study of the novel tuned mass damper with inerter which enables changes of inertance, Journal of Sound and Vibration 404 (2017) 47–57.

[29] P. Brzeski, P. Perlikowski, Effects of play and inerter nonlinearities on the performance of tuned mass damper, Nonlinear Dynamics 88 (2017) 1027–1041.

[30] F. C. Wang, H. Chan, Vehicle suspensions with a mechatronic network strut, Vehicle System Dynamics 49 (2011) 811–830.

[31] L. Pires, M. Smith, N. Houghton, R. McMahon, Design trade-offs for energy regeneration and control in vehicle suspensions, International Journal of Control 86 (2013) 2022–2034.

[32] A. Gonzalez-Buelga, L. Clare, S. Neild, J. Jiang, D. Inman, An electromagnetic inerter-based vibration suppression device, Smart Materials and Structures 24 (2015) 055015.

[33] F. C. Wang, W. Su, C. Chen, Building suspensions with inerters, Proceedings of the Institution of Mechanical Engineers, Part C, Journal of Mechanical Engineering Science 224 (2010) 1650–1666.

[34] K. Ikago, K. Saito, N. Inoue, Seismic control of single-degree-of-freedom structure using tuned viscous mass damper, Earthquake Engineering and Structure Dynamics 41 (2012) 453–474.

[35] H. Garrido, O. Curadelli, D. Ambrosini, Improvement of tuned mass damper by using rotational inertia through tuned viscous mass damper, Engineering Structures 56 (2013) 2149–2153.

[36] I. Lazar, S. Neild, D. Wagg, Using an inerter-based device for structural vibration suppression, Earthquake Engineering and Structure Dynamics 43 (2014) 1129–1147.

[37] S. Y. Zhang, J. Z. Jiang, S. Neild, Passive vibration control: a structure-immittance approach, Proceedings of Royal society, part A 473.

[38] L. Marian, A. Giaralis, Optimal design of a novel tuned mass-damper-inerter (tmdi) passive vibration control configuration for stochastically support-excited structural systems, Probabilistic Engineering Mechanics 38 (2014) 156–164.

[39] L. Marian, A. Giaralis, The tuned mass-damper-inerter for harmonic vibrations suppression, attached mass reduction, and energy harvesting, Smart structures and systems 19 (2017) 665–678.

[40] A. Giaralis, A. Taflanidis, Optimal tuned mass-damper-inerter (tmdi) design for seismically excited mdof structures with model uncertainties based on reliability criteria, Structural Control and Health Monitoring 25 (2018) 10.1002/stc.2082.

[41] D. Pietrosanti, M. D. Angelis, M. Basili, Optimal design and performance evaluation of systems with tuned mass damper inerter (tmdi), Structural Control and Health Monitoring 46 (2017) 1367–1388.

[42] Y. Shen, L. Chen, Y. Liu, X. Zhang, Modeling and optimization of vehicle suspension employing a nonlinear fluid inerter, Shock and Vibration (2016) 2623017.

[43] G. Warburton, Optimum absorber parameters for various combinations of response and excitation parameters, Earthquake Engineering and Structural Dynamics 10 (1982) 381401.

[44] S. Y. Zhang, J. Z. Jiang, S. Neild, Optimal configurations for a linear vibration suppression device in a multi-storey building, Structural Control and Health Monitoring 24 (2016) 10.1002/stc.1887.